

# Influence of distinct tool pin geometries on aluminum 8090 FSW joint properties

Harikrishna Rana<sup>1,a\*</sup>, Vivek Patel<sup>2,b</sup>, Gianluca Buffa<sup>1,c</sup>, Livan Fratini<sup>1,d</sup>  
and Rosa Di Lorenzo<sup>1,e</sup>

<sup>1</sup>Department of Engineering, University of Palermo, Viale Delle Scienze, 90128 Palermo, Italy

<sup>2</sup>Department of Engineering Science, University West, 46186, Trollhättan, Sweden

<sup>a</sup>harikrishnasinh.rana@unipa.it, <sup>b</sup>vivek.patel@hv.se, <sup>c</sup>gianluca.buffa@unipa.it,

<sup>d</sup>livan.fratini@unipa.it, <sup>e</sup>rosa.dilorenzo@unipa.it

**Keywords:** Friction Stir Welding, Aluminum, Pin Profile

**Abstract.** Aluminum Lithium alloys are recuperating substantial interest from automotive and aerospace industries owing to their extraordinary specific strength as compared to conventional aluminum (2xxx, 6xxx, and 7xxx) alloys. The goal of the present investigation is to study AA 8090 joints produced with the unique solid-state welding technique friction stir welding (FSW). Tool pin profile induces remarkable influence on friction and further plastic deformation during FSW. Therefrom, the influences of three distinct but constant dynamic area conditioned tool pin geometries namely, square trapezoidal, hexagonal trapezoidal, and threaded taper on the resulting material flow patterns, mechanical properties, and the microstructure have been studied and discussed in detail. The FSW joint produced with hexagonal trapezoidal pin geometry delivered the highest joint resistance owing to grain refinement and almost flawless microstructure.

## Introduction

The development of 2<sup>nd</sup> generation Al-Li alloys had stirred the aerospace and automotive industries by offering 2-8 % lesser density than most conventional 2000 and 7000 series aluminum alloys. This novel Al-Li alloy not only offers the potential for substantial weight saving in structural components but high specific strength and corrosion resistance [1]. Furthermore, these alloys possess excellent mechanical properties owing to a wide variety of precipitates present in the microstructure, depending on the heat treatment condition [2]. However, the joining of these alloys by conventional arc welding methods is problematic due to the defects associated viz., porosity, hot cracking, and evaporative loss of Li [3].

FSW is an innovative solid-state joining technology wherein such fusion-related defects can be eradicated up to a certain extent [4]. During FSW joining is carried out by the plastic material flow engendered by hot–shearing action engendered by rotating non-consumable tool. Until now, the majority of investigations in FSW of Al-Li alloy are focused on the influences of various process parameters like tool rotation (TR) and tool traverse (TT) speeds on microstructure and resulting mechanical properties [3, 5]. Lertora et al.[5] have discussed the role of revolutionary pitch (RP) on joint resistance and the fatigue strength of the prepared joint. They reported enhanced properties with lower RP values owing to defect-free microstructure obtained by higher specific thermal contribution (STC). As reported by Alam et al. [6], apart from the machine parameters like TR and TT, tool pin geometry plays a vital role in the material flow characteristics, STC and so the resulting microstructure. However, hardly a few researchers have reported the role of pin geometry on the microstructure and properties of FSW joints.

For a rotating body, eccentricity is related to the dynamic orbit generated due to the disparity between the two centers. As FSW is concerned, polygonal pin geometries such as square or hexagonal can be related to eccentricity. During tool stirring such eccentricity incorporates

incompressible material to hover around the pin profile. As reported by Thomas et al. [7], the eccentricity of the rotating body can be associated with the dynamic volume of the pin profile owing to different centers. The volume of the engendered WZ at the end of FSW is basically similar to the dynamic volume of pin geometry. The trajectory of the material flow is majorly decided by the ratio of static to dynamic volume. In this regard, the present study is aimed at investigating material flow, microstructure, and mechanical properties resulting from various tool pin profiles possessing constant dynamic volume.

### Experimental Design

Aluminum alloy 8090 (Li 2.7%, Mg 0.6-1.3%, Cu 1-1.6 %, Fe 0.6%, Si 0.2 %, Mn 0.1%, Cr 0.1, Al bal%) plates with dimensions: 100mm×50mm×6mm were used as substrates (Supplier: Migliari Alluminio srl). All the experiments were conducted on fully automatic ESAB (LEGIO) FSW machine. Butt joints were produced using three different M3 (Molybdenum enriched high-speed steel) tools as depicted with their geometries in Fig. 1. The milling center was used to manufacture polygonal pin profiles (Tool 1 & 2) whereas the turning center was used to manufacture taper threaded cylindrical pin profiles (Tool 3).

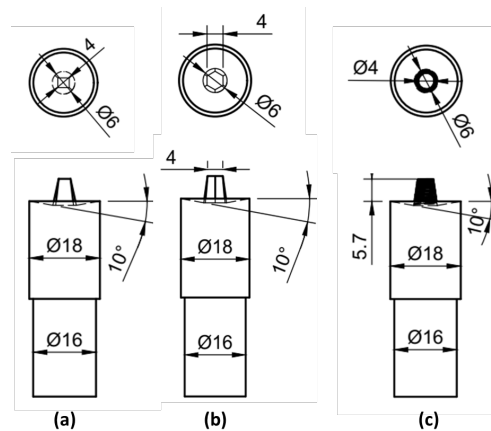


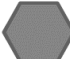





Figure 1: Tool geometries: (a) Square Trapezoidal pin (b) Hexagonal Trapezoidal pin (c) Tapered Threaded cylindrical pin<sup>1</sup>

All the experiments were carried out using the tool with the same shoulder diameter (SD) and pin length (PL) i.e. 18 mm and 5.9 mm, respectively. The static and dynamic conditions of distinct pin geometries are tabulated in Table 1. The faces of polygonal pins as well as conical pins were designed in accordance to have the same dynamic area conditions during FSW. Static dimensions are the actual dimensions of the pin which were used for the tool manufacturing. Dynamic dimensions are those which result during the stirring action (tool rotation). Dynamic volume decides the swept volume of the WZ. Apart, the TR, TT, and tilt angle were optimized with previous feasibility trials and kept constant for each tool pin geometry viz., 1700 rev. min<sup>-1</sup>, 50 mm min<sup>-1</sup>, and 3° respectively. Three FSW specimens were prepared with each welding condition as tabulated with their specimen IDs in Table 2. The temperature was also monitored during FSW for each specimen through mounting the K-type thermocouple 3mm beneath and 15 mm sideway from centre of weld line.

Table 1: Details of tool pin design on static and dynamic area conditions\*

Pin Profile	Pin Dimensions [mm]	V <sub>s</sub> [mm <sup>3</sup> ]	V <sub>d</sub> [mm <sup>3</sup> ]	V <sub>d</sub> / V <sub>s</sub>	Static area condition	Dynamic area condition
Square Trapezoidal	PL: 5.9 a: 4	115.52		1.16		
Hexagonal Trapezoidal	PL: 5.9 a: 6	126.57	134.4	1.06		
Tapered Threaded cylindrical	PL: 5.9 Dr:6 Dt:4	130.24		1.03		

\*PL: Pin Length, Dr: Root Diameter, Dt: Tip Diameter , a: No. of faces/sides of polygonal pin

Table 2: Specimen IDs with their FSW conditions

Specimen ID	Pin Geometry	Tool Rotation [rev minute <sup>-1</sup> ]	Tool Traverse [mm minute <sup>-1</sup> ]	Tilt Angle
A	Square Trapezoidal			
B	Hexagonal Trapezoidal	1700	50	3°
C	Tapered Threaded cylindrical			

Microstructural examination specimens were sectioned perpendicular to the welded joint line as exhibited in Fig. 2. They were further polished up to 1µm finish as per the standardized specimen preparation process. Each specimen was further etched with Keller’s etchant (1 ml HF + 1.5 ml HCL + 2.5 ml HNO<sub>3</sub> + 95 ml DI water) [8]. The WZ area, grain morphologies, gross microstructure, and defects were analyzed with optical macro and microscopy.

Specimens prepared with each welding condition were sliced with a wire-cut electro-discharge machine (EDM) for extracting tensile specimens with dimensions according to ASTM E8M-04 guidelines.

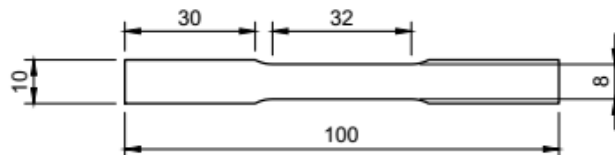


Figure 2: Tensile Specimen Schematic

**Results And Discussion**

Thermal Impact. Table 3 summarizes the effective pin and shoulder area, peak temperatures during FSW, and area of WZ resulting from different pin geometries. Therefrom, it is seen that specimen A, which was prepared with square trapezoidal pin geometry displayed the largest WZ area followed by specimen B and specimen C. This can be attributed to the different heat inputs generated by different pin geometries. The peak temperatures for the square trapezoidal pin geometry specimens are also the highest among the other geometry. The amount of frictional heat engendered during FSW can be attributed to two different interactions. First, the interaction between the tool pin and substrate material wherein the pin geometry makes the difference. Secondly, the shoulder-substrate interaction inducts a major amount of heat.

*Table 3: Specimens Id wise tool geometry dimensions, peak temperature, and WZ area*

Specimen Id	Pin Geometry	Effective pin surface area [mm <sup>2</sup> ]	Effective shoulder surface area [mm <sup>2</sup> ]	Peak Temp [°C]	Standard Deviation	Weld Zone Area [mm <sup>2</sup> ]
A	Square Trapezoidal	119.56	236.16	393	+4, -3	47.12
B	Hexagonal Trapezoidal	124.49	231.27	384	+2, -3	38.58
C	Tapered Threaded cylindrical	128.57	229.68	363	+3, -4	29.75

It is important to notice that the effective shoulder area is higher than that of the pin for all the tools. Further, the effective shoulder area reduces as the number of faces is increased from 4 for square geometry to 6 for hexagonal geometry to infinite faces for cylindrical geometry. Conversely, the effective pin interaction area upsurges as the number of faces increases. Since the shoulder friction contribution to total heat input is much higher than the pin, the square pin geometry specimens exhibited the highest peak temperatures as compared to hexagonal and taper cylindrical pin geometry specimens. Accordingly, as the resulting WZ area is highly reliant on the peak temperature during FSW, the square trapezoidal pin geometry specimens exhibited the highest WZ area. Apparently, it is now well understood that WZ is the reflection of the tool pin geometry clubbed with the temperature history during FSW.

Micro and Macrostructural characterization. Fig. 3 exhibits macro and microstructural zones developed at distinct locations of the prepared FSW joints with distinct pin geometries. From the macrostructure, an interesting observation can be made about the material flow for all the samples. Therefrom, complete penetration of the tool pin was evident for all the specimens. Moreover, interesting observations can be made with distinct material flow patterns pertaining to each specimen. The tool substrate interaction generally happens in two areas namely, the shoulder interaction area and the pin interaction area. The material flow that happened at the top of WZ is attributable to shoulder interaction while for the middle and the bottom region, pin interaction. The microstructure of all the specimens has revealed the microstructural transition from WZ to thermos mechanically affected zone (TMAZ), and TMAZ to heat affected zone (HAZ). The WZ of all the specimens were characterized with finer grain structure which can be attributed to dynamic recrystallization while FSW [4, 9-11].

As reported by Elangovan et al. [12] polygonal pin profile produces the pulsating action whereas no such pulsation is produced with cylindrical or tapered cylindrical pin geometries. The number of pulses/second considerably contributes to the amount of plastic deformation and heat generation. The number of pluses can be calculated by multiplying the TR by the number of flat faces. Hence for a square pin, it is 113 pulses/second, while it is 170 pulses/second for the hexagonal trapezoidal pin. A higher number of pulses/second generates higher turbulence while stirring which ensues in finer grain structure along with well-distributed fine precipitates [9]. The grain size comparison is portrayed in Fig. 3(d) for each sample.

The unprocessed substrate displayed a grain size of ~120 μm mostly shaped like a pancake as plates were obtained from a rolled stock of AA 8090. These grains were refined by almost 90-95% in the WZ of prepared FSW joint specimens. Such extreme grain refinement in WZ can be reportedly attributed to several DRX mechanisms [13]. Su et al. [13] have reported several grain sizes in different portions of WZ in multi-pass FSP ensuing from discontinuous DRX mechanism. As discussed earlier, since the WZ grains of joints prepared with polygonal pins experience multiple pulses engendering tremendous plastic deformation and turbulence, a discontinuous DRX mechanism can be opted in the present case. On the one hand, the joints prepared with polygonal pins exhibited more grain size variations in WZ as compared to threaded taper cylindrical pins.

This has resulted due to intermittent interaction of the pin's multiple faces and substrate during FSW using polygonal pins. This intermittent interaction further creates turbulence and leads to non-uniform grain deformation. On the other hand, the joints prepared with threaded taper cylindrical pin exhibited finely distributed grain structures with less variation.

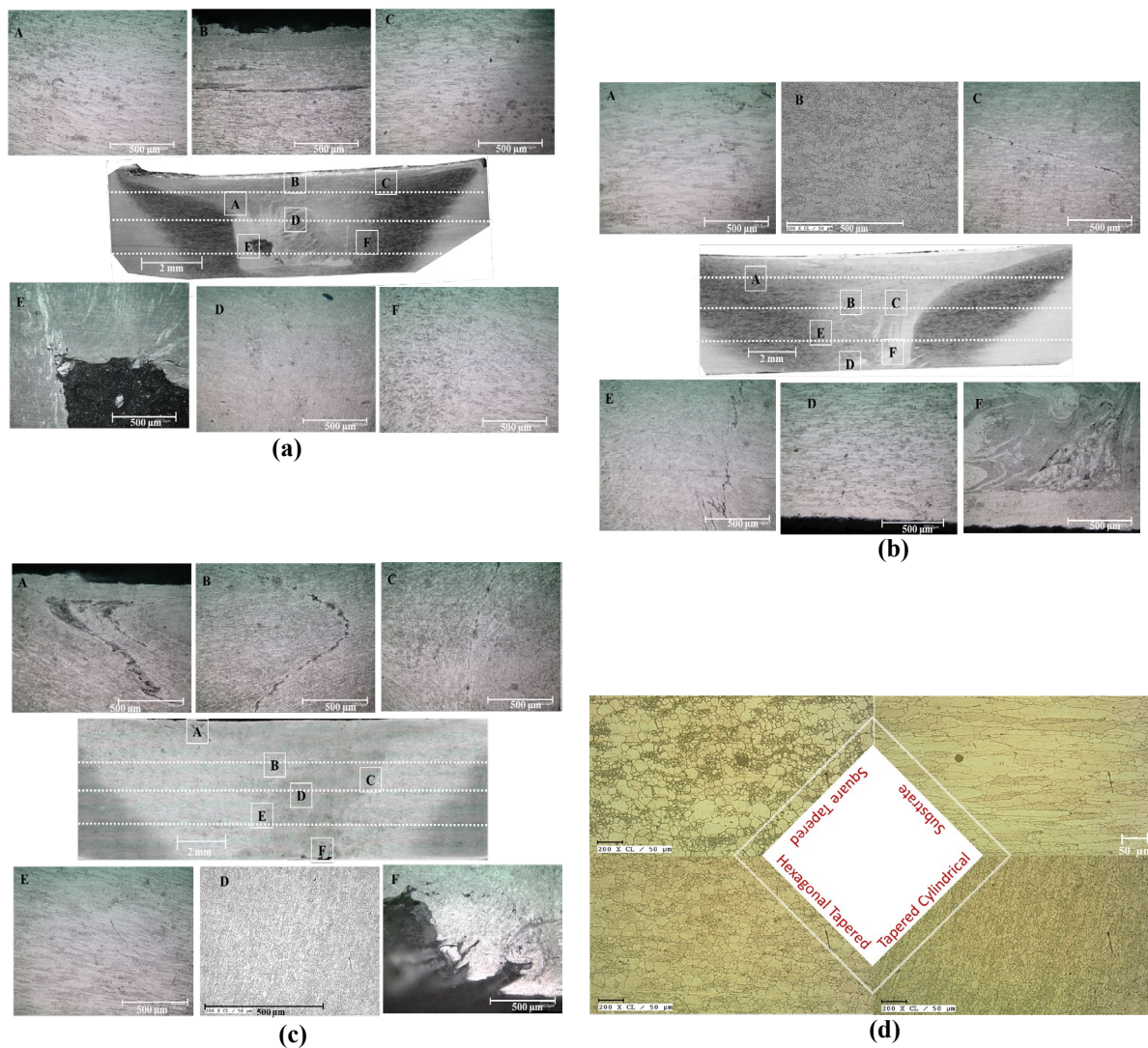


Figure 3: Macro and Microstructures of the specimens joined with different pin geometries: (a) Square Trapezoidal Pin (b) Hexagonal Trapezoidal Pin (c) Tapered Threaded cylindrical Pin (d) Grain structure comparison of all the specimens with parent metal

It is noteworthy that with an increase in the number of faces of the polygon the grain size variation diminishes as evident with the hexagonal pin geometry. As described in section 2.1 the dynamic volume of all the pin geometries was kept the same. For more regular shapes like cylindrical geometry, there is less or no disparity between the static and dynamic volume and so their ratio is unity. Specifically, in the case of polygonal pin geometries, this disparity increases with a reduction in the number of faces. For instance, the ratio is maximum in the case of square pin geometry, whereas it gets close to unity with hexagonal pin geometry (see Table 1). So, when the number of faces is increased from 4 to 6 the pin geometry gets closer to cylindrical geometry and creates less turbulence during FSW and deforms grain more homogeneously. Although the lowest grain sizes of 3-8 $\mu$ m were noticed with the hexagonal trapezoidal pin geometry, the

threaded tapered cylindrical pin exhibited slightly larger (5-8 $\mu\text{m}$ ) but more uniform grains in the WZ. The WZ of the square threaded specimen exhibited the largest grain size of 4-15 $\mu\text{m}$ .

Apart from that, the specimen processed with a hexagonal trapezoidal pin exhibited almost defect-free WZ (see Fig. 3(b)). Whereas the WZ of the square trapezoidal pin specimen was characterized with a large wormhole cavity, the WZ of the taper cylindrical pin specimen was identified with a small cavity at the bottom as exhibited in Fig. 3(a) and (c) respectively. As indicated earlier the pulsating action engendered by polygonal pin multiple faces fosters turbulence while stirring in FSW. As the number of faces in the pin decreases a larger material void is created intermittently around the pin which gives rise to the cavity or tunnel in the WZ. However, with increases in the number of faces, the geometry becomes alike circular and so in absence of such intermittent material flow and void generation, the defects are minimized.

Tensile test behavior. All the specimens were subjected to tensile testing as per ASTM E8M-04 guidelines. The joint resistance results along with joint efficiencies are compared for all the specimens through the chart portrayed in Fig. 4.

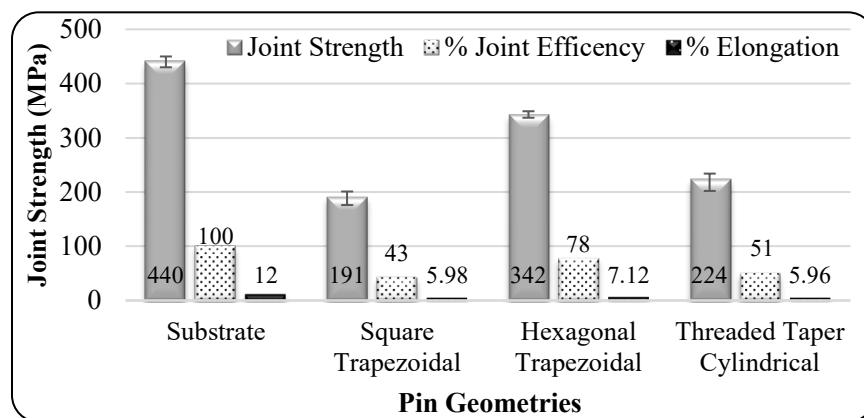


Figure 4: Tensile properties comparison of all specimens

Specimen B which was joined with hexagonal trapezoidal pin geometry delivered the highest joint resistance of 342 MPa and remarkable joint efficiency of ~78 %. It is noteworthy that the % elongation was almost 60% that of the substrate. Such remarkable joint properties were observed owing to highly refined grain structure in the WZ characterized by flawless microstructure. The highest grain refinement ensued from the pulsating action of hexagonal tool faces offers a higher grain boundary area which in due course hinders the dislocation motion. This hindrance not only increases joint resistance but also increases other properties like hardness and fatigue resistance [14]. Apart, precipitation strengthening offered by major precipitates like  $\text{Al}_2\text{CuLi}$ ,  $\text{Al}_3\text{Zr}$ , and  $\text{Al}_3\text{Li}$  are also attributable for heightened properties [3]. Moreover, as WZ of specimen B possessed different sizes of grains, the larger grains aided in boosting the % elongation up to 60 %. As far as the other two cases are concerned, specimen A which was joined with square pin geometry delivered meager joint resistance owing to a large cavity in the center of the WZ, whereas specimen C produced with a threaded taper pin exhibited moderate joint resistance owing to the cavity at the bottom of the joint.

Apart from the joint resistance results, it is important to consider the location of the fracture for the tested specimens. The location of the fracture for each tensile specimen is depicted by white arrows in Table 5.

*Table 5: Tensile test fracture specimens displaying fracture location for all the welding conditions*

Specimen ID.	Fractured specimen: Location	Fractured Specimen: Side view
A		
B		
C		

Therefrom, it can be observed that except for specimen B, all the specimens fractured from the center of the WZ. The WZ of specimens processed with a square trapezoidal pin and threaded taper cylindrical pin was identified with cavity and tunnel defects at the center/ bottom which may be the preferential site for the crack initiation and further growth leading to the fracture. However, it was interesting to notice that the specimens prepared with hexagonal pin fractured from the TMAZ/HAZ interface. This can be understood by the two circumstances. Firstly, the WZ of these specimens was characterized with immaculate microstructure. Secondly, as depicted in section E of Fig. 3 (ii) the transition zone of the TMAZ/HAZ was characterized with the transition of the fine grain to a larger grain structure. As the WZ possesses a highly refined grain structure, the HAZ region becomes the weak spot and a preferential site for crack initiation and further growth.

### Conclusions

The present investigation described the influences of distinct pin geometries on thermal characteristics, microstructural characteristics, and mechanical properties of AA 8090 FSW joints. Further, the following conclusions were extracted from the investigation:

- The tool pin geometry significantly influences the heat generation, microstructural features like weld zone size, grain size, grain morphology, and mechanical properties like joint resistance and joint elongation.
- Square trapezoidal pin geometry generated the highest heat input with a peak temperature of 395 °C even though possessing the lowest pin face area. However, this geometry offers the highest effective shoulder interaction area and the shoulder's frictional heat contribution is greater than the pin's contribution. This pin geometry delivered the specimen with the highest WZ area owing to the highest peak temperature.
- The pulsating action of the polygonal pin characterized by the number of pulses/second contributes greatly to the grain refinement and distribution pattern during FSW. Specimen prepared with the hexagonal trapezoidal pin exhibited the finest grains owing to the turbulence created by the highest number of pulses/second. Simultaneously, the lower number of pulses creates intermittent material voids around the pin while tool stirring which is responsible for the greater non-uniformity in the grain sizes and the defects generation.
- The specimens joined with hexagonal trapezoidal pin exhibited the highest joint resistance along with the highest elongation in line with the grain size results. The rare combination of the high joint resistance and elongation was possible owing to a moderate disparity in the grain sizes in the weld zone of these specimens, wherein larger grains promoted the elongation. Only these specimens fractured from the TMAZ/HAZ interface owing to a large grain size gradient at the interface and a weak HAZ region characterized by larger grains.

## References

- [1] Y. Tao, D. Ni, B. Xiao, Z. Ma, W. Wu, R. Zhang, Y. Zeng, Origin of unusual fracture in stirred zone for friction stir welded 2198-T8 Al-Li alloy joints, *Materials Science and Engineering: A* 693 (2017) 1-13. <https://doi.org/10.1016/j.msea.2017.03.079>
- [2] B. Decreus, A. Deschamps, F. De Geuser, P. Donnadieu, C. Sigli, M. Weyland, The influence of Cu/Li ratio on precipitation in Al-Cu-Li-x alloys, *Acta Mater.* 61(6) (2013) 2207-2218. <https://doi.org/10.1016/j.actamat.2012.12.041>
- [3] H. Liu, Y. Hu, C. Dou, D.P. Sekulic, An effect of the rotation speed on microstructure and mechanical properties of the friction stir welded 2060-T8 Al-Li alloy, *Mater. Charact.* 123 (2017) 9-19. <https://doi.org/10.1016/j.matchar.2016.11.011>
- [4] H. Rana, D. Campanella, G. Buffa, L. Fratini, Dissimilar titanium-aluminum skin-stringer joints by FSW: process mechanics and performance, *Mater. Manuf. Process* (2022) 1-14. <https://doi.org/10.1080/10426914.2022.2116044>
- [5] E. Lertora, C. Gambaro, AA8090 Al-Li alloy FSW parameters to minimize defects and increase fatigue life, *International Journal of Material Forming* 3(1) (2010) 1003-1006. <https://doi.org/10.1007/s12289-010-0939-1>
- [6] M.P. Alam, A. Sinha, Fabrication of third generation Al-Li alloy by friction stir welding: a review, *Sādhanā* 44(6) (2019) 1-13. <https://doi.org/10.1007/s12046-019-1139-4>
- [7] W. Thomas, E. Nicholas, Friction stir welding for the transportation industries, *Mater. Des* 18(4-6) (1997) 269-273. [https://doi.org/10.1016/S0261-3069\(97\)00062-9](https://doi.org/10.1016/S0261-3069(97)00062-9)
- [8] G.F. Vander Voort, S.R. Lampman, B.R. Sanders, G.J. Anton, C. Polakowski, J. Kinson, K. Muldoon, S.D. Henry, W.W. Scott Jr, ASM handbook, *Metallography and microstructures* 9 (2004) 44073-0002. <https://doi.org/10.31399/asm.hb.v09.9781627081771>
- [9] V.V. Patel, V. Badheka, A. Kumar, Effect of polygonal pin profiles on friction stir processed superplasticity of AA7075 alloy, *J. Mater. Process. Technol.* 240 (2017) 68-76. <https://doi.org/10.1016/j.jmatprotec.2016.09.009>
- [10] H. Rana, V. Badheka, Elucidation of the role of rotation speed and stirring direction on AA 7075-B4C surface composites formulated by friction stir processing, *Proceedings of the Institution of Mechanical Engineers, Part L: Journal of Materials: Design and Applications* (0) (2017) 1-18. <https://doi.org/10.1177/1464420717736548>
- [11] H. Rana, V. Badheka, A. Kumar, A. Satyaprasad, Strategical parametric investigation on manufacturing of Al-Mg-Zn-Cu alloy surface composites using FSP, *Mater. Manuf. Process* 33(5) (2018) 534-545. <https://doi.org/10.1080/10426914.2017.1364752>
- [12] K. Elangovan, V. Balasubramanian, Influences of pin profile and rotational speed of the tool on the formation of friction stir processing zone in AA2219 aluminium alloy, *Materials Science and Engineering: A* 459(1-2) (2007) 7-18. <https://doi.org/10.1016/j.msea.2006.12.124>
- [13] J.-Q. Su, T.W. Nelson, C.J. Sterling, Friction stir processing of large-area bulk UFG aluminum alloys, *Scr. Mater* 52(2) (2005) 135-140. <https://doi.org/10.1016/j.scriptamat.2004.09.014>
- [14] V. Patel, W. Li, A. Vairis, V. Badheka, Recent development in friction stir processing as a solid-state grain refinement technique: microstructural evolution and property enhancement, *Critical Reviews in Solid State and Materials Sciences* 44(5) (2019) 378-426. <https://doi.org/10.1080/10408436.2018.1490251>